Geophys. J. Int. (2004) **159,** 721–733 doi: 10.1111/j.1365-246X.2004.02450.x

A global survey of stress orientations in subducting slabs as revealed by intermediate-depth earthquakes

Po-Fei Chen,* Craig R. Bina and Emile A. Okal

Department of Geological Sciences, Northwestern University, Evanston, IL 60208, *USA*

Accepted 2004 July 22. Received 2004 July 7; in original form 2004 January 15

SUMMARY

We examine a variety of mechanisms that have been proposed as contributors to the stress fields expressed as intermediate-depth seismicity in subducting slabs. To this end, we study principal stress orientations for a global data set of 1900 intermediate-depth focal solutions, determining the patterns of events characterized primarily by downdip compression, downdip tension, or neither. In regions dominated by downdip principal stresses, we find that conjugate stress axes exhibit preferential slab-normal orientations. Furthermore, we observe a clear trend of thermal control, in which colder slabs exhibit greater components of downdip compression while warmer slabs display greater downdip tension. In those regions not dominated by downdip principal stresses, a significant number of events exhibit lateral stresses in the form of subhorizontal principal axes in the plane of the slab. We conclude that the evidently complementary roles played by lithospheric age and subduction rate in constraining stress regimes support thermomechanical and petrological buoyancy models for control of intermediate-depth stresses. Moreover, observed lateral stresses support the traditional model of a squeezed ping-pong ball and stress patterns overall are consistent with some influence by reactivated fossil faults.

Key words: intermediate-depth seismicity, stress orientation, subduction earthquakes.

1 INTRODUCTION

The purpose of this study is to provide a new appraisal of the various mechanisms proposed as contributors to stress release in intermediate-depth earthquakes (with foci between 70 and 300 km). We are motivated to carry out a new study in a field with a long history of investigations (e.g. Isacks & Molnar 1971; Davies 1980; Fujita & Kanamori 1981; Apperson & Frohlich 1987; Vassiliou & Hager 1988; Zhou 1990) by three recent developments: the constant updating of the earthquake database through improvements in location techniques (Engdahl *et al.* 1998) and centroid-moment tensor data sets (Dziewonski *et al.* 1983, and subsequent quarterly updates); the design of a new visualization technique for large data sets of focal mechanisms providing unbiased optimization of regional directions of principal stresses (Chen *et al.* 2001a); and progress in the understanding of the mineralogical fabric of slabs as a function of pressure and temperature (e.g. Bina *et al.* 2001).

This paper first presents a review of several previous models for the geometry of stress release in intermediate-depth earthquakes. A database of 1900 focal solutions is then assembled and organized in systems of slab-oriented coordinates for 50 distinct geographic segments covering all of the subduction zones of the Earth. This allows the formal characterization of each earthquake as downdip compressional (hereafter DP), downdip tensional (DT) or not aligned downdip (ND). In turn, individual regions can be formally defined as dominated or not by downdip stresses, based on their relative populations of DP, DT and ND events.

The previously published models are then critically analysed and their predictions evaluated in the context of the geometrical parameters of stress release in each of the 50 regions. We conclude that lithospheric age and subduction rate play complementary roles in controlling downdip stress patterns at intermediate depths, in agreement with thermomechanical and petrological buoyancy models. Lateral stresses in strongly curved arcs are consistent with the traditional model of a squeezed ping-pong ball and seismic stress patterns are also consistent with influence by reactivated fossil faults.

2 PUBLISHED MODELS FOR STRESS REGIMES IN SUBDUCTING SLABS

2.1 The thermomechanical model

In the very first global analysis of the focal geometries of non-shallow earthquakes, Isacks & Molnar (1971) made the fundamental observation that intermediate-depth earthquakes exhibit downdip compression in regions where seismicity continues to greater depths (∼500 km) and downdip extension where a marked seismicity gap separates the deepest seismicity, or where deep seismicity is entirely absent. This was generally interpreted as the result of interaction

*Now at: Central Weather Bureau, 64 Kung Yuan Road, Taipei 10039, Taiwan.

between: (i) the negative buoyancy of cold, hence dense, slabs; (ii) frictional forces expressing shear stresses on the two sides of the downgoing slabs; and (iii) resistant forces expressing inhibition of slab penetration into the lower mantle, as a result of increasing viscosity and/or chemical changes at the bottom of the transition zone (Richter 1979).

However, the consistency of observations predicted by the thermomechanical model has been questioned by Green & Houston (1995), who noted that those subduction zones with continuous seismicity to the greatest depths and DP events at intermediate depths (such as Tonga, the Solomon Islands, Japan, and much of the Kuriles) still exhibit a significant minimum in seismic activity around 350 km. Despite detailed studies of several of these regions (Zhou 1990; Lundgren & Giardini 1992), it remains hard to bring the argument to a clear verdict, given the complexity of their stress regimes and the difficulty of visualization of their focal mechanisms.

2.2 Petrological model of buoyancy forces

Recent studies (Bina 1997; Yoshioka *et al.* 1997) have proposed that perturbations of phase transition boundaries resulting from thermal anomalies in slabs are major contributors to their stress fields. The latter can be modelled by considering contributions from thermal contraction of the slab, perturbed boundaries of phase transitions and the possible presence of a wedge of metastable olivine (Goto *et al.* 1983, 1985, 1987; Bina 1996, 1997; Yoshioka *et al.* 1997). Guest *et al.* (2003) have recently proposed that accumulated volumetric stresses from successive phase changes can generate slab stress fields that are qualitatively consistent with observed seismicity and exceed in magnitude stresses arising from buoyancy forces.

In the case of deep earthquakes, Bina *et al.* (2001) successfully modelled stress orientations, and the distribution and cessation of seismicity, thus confirming the major role of these petrological buoyancy forces on slab stress regimes. This suggests investigating whether or not such thermally induced forces also control stress fields at intermediate depths. To this end, we will consider regions with dominant downdip stresses and make use of the concept of slab thermal parameters (Kostoglodov 1989; Kirby *et al.* 1991) to investigate the performance of this model, which we will refer to as the petrological model.

2.3 The ping-pong model

The arcuate, oceanward convex, geometry of the majority of ocean trenches was noted early on by Frank (1968). Their curvature can be quantified through the concept of the radius of curvature (RC) angle, defined as half the vertex angle of the cone subtended at the centre of the Earth by the small circle describing the arc on the surface of the planet (Tovish & Schubert 1978). Frank (1968) further inferred that, for an inextensible spherical shell, the RC angle should equal half the dip angle of the subduction, as in the case of a squeezed[1] ping-pong ball. This condition ensures that the total curvature of the slab surface remains zero, creating no membrane stress (e.g. Creager *et al.* 1995). Regions that deviate significantly from this relationship would experience substantial lateral stresses (Isacks & Molnar 1971; Bevis 1986). In this framework, we shall investigate whether regional stress patterns associated with features of slab geometry can be predicted from Frank's model, which, for brevity, we call the ping-pong model.

[1] We prefer the adjective 'squeezed' to the commonly used 'punctured' when describing the familiar deformation of a ping-pong ball, as it usually does not involve a rupture of the shell.

2.4 Double seismic zones

Ever since the observation by Sykes (1966) in the Southern Kuriles, it has been known that several subduction zones exhibit double seismic zones in the depth range 65 to 185 km, with the upper layer in downdip compression and the lower one in downdip tension (e.g. Kuriles, Kao & Chen 1994; Northern Japan, Umino & Hasegawa 1975). Stresses associated with phase changes (Veith 1974; Kao & Liu 1995), unbending of the slab (Engdahl & Scholz 1977; Tsukahara 1980; Samowitz & Forsyth 1981; Kawakatsu 1985), sagging of the plate (Sleep 1979) and thermoelasticity (House & Jacob 1982; Hamaguchi *et al.* 1983) all have been proposed as a possible origin of double seismic zones. In addition, Yamasaki & Seno (2003) have proposed that intermediate-depth earthquakes may arise from a mechanism involving dehydration embrittlement; calculated dehydration loci for subducted oceanic lithosphere would form two-layered structures that are consistent with observed double seismic zones. Regardless of which of those mechanisms are physically plausible, they would have to accommodate the non-ubiquitous character of double seismic zones and contribute to the stress regime only over a small range of intermediate depths.

2.5 Fujita and Kanamori's (FK) model

Fujita & Kanamori (1981) conducted a global survey of then-published focal mechanisms between depths of 70 and 230 km, and suggested that the stress in the slab is controlled by its age and by the rate of convergence at the trench. In old and slow slabs, their sinking, as a result of thermal contraction, tends to be faster than surface convergence and hence DT stresses are expected inside the slab. Young and fast slabs are the exact opposite and DP stresses would be expected. Old and fast, or young and slow, slabs are expected to exhibit mixed stress patterns. These authors also pointed out that double seismic zones tend to occur in old and fast slabs, whereas young and slow ones feature stress patterns varying along strike (giving rise to a so-called stress-segmented zonation of the subduction). Fujita and Kanamori also acknowledged that the downdip extension observed in the young and fast Nazca slab runs contrary to the model predictions. To explain this observation, they invoked the loading of overriding lithosphere as the dominant force acting on that slab. We now understand (Engebretson & Kirby 1992) that the bottom of the Nazca slab features a large age discontinuity, which can result in a strong mechanical pull from the old, deep section of the slab on its shallow and younger counterpart.

2.6 Temporal variation of slab stress as a result of large interplate thrust events

Astiz *et al.* (1988) and Lay *et al.* (1989) proposed that one contributor to slab stress regimes at intermediate depths arises from dynamic stresses, i.e. the locking and unlocking of subducting slabs with overriding plates during the cycle of large interplate events. According to their model, DT intermediate-depth earthquakes observed prior to a large interplate thrust earthquake either decrease in frequency, or completely convert to DP events, shortly after the occurrence of the large thrust shock. This pattern was observed in several cases, notably for the 1957 Aleutian, 1960 Chile and 1963 Kuriles earthquakes (Lay *et al.* 1989).

2.7 Intermediate-depth earthquakes as caused by reactivation of fossil faults

Jiao *et al.* (2000) observed that an asymmetric fault system (with dip angles deviating from 45°) with a strike parallel to the trench, persists down to 450 km in Tonga and the Kuriles, resembling the fault geometry of outer-rise earthquakes. They thus suggested that intermediate-depth earthquakes are caused by the reactivation of pre-existing faults. Although this issue is more related to the origins of intermediate-depth seismogenesis rather than to that of stress regimes in slabs, our compilations are capable of testing the legitimacy of this hypothesis, because stress orientations are related to fault geometry.

In addition, slab stresses can be generated under specific situations pertaining to local conditions in individual slabs, such as the lateral propagation of a tear under in-slab tensional stresses, as described in the case of Vanuatu by Yoshioka & Wortel (1995).

As a final note, we stress that not all these models are directly comparable: for example, the thermomechanical model (1), the petrological model (2), the double seismic zone model (4), the FK model (5) and the slab coupling model (6) all address the nature of downdip stresses, whereas the ping-pong model (3) involves horizontal stresses. The contributions suggested from the thermomechanical, petrological and FK models, are all expected to be universal, whereas the ping-pong, double seismic zones and slab coupling models apply only in regions offering specific features in their slab geometry or kinematics. Similarly, the variation in stress induced by slab coupling shortly after great thrust events is expected to be transient, as opposed to universal in time. The age of the slab and the rate of convergence have the same sign of contribution in the petrological model (old and fast slabs are colder), but they are competitive factors in the FK model. The effects of slab coupling and the mechanisms for double seismic zones may affect the shallower portion of the intermediate-depth range, whereas the petrological forces may contribute more to the deeper portion of the slab through variations in the depths of phase transitions.

3 METHODOLOGY AND DATA SETS

The study of the geometry of stress release during intermediate-depth earthquakes in the context of slab geometry requires the definition of individual segments of subduction zones where the latter can be deemed homogeneous. To this end, and as illustrated in the case of Tonga–Kermadec on Fig. 1, we consider the full data set of

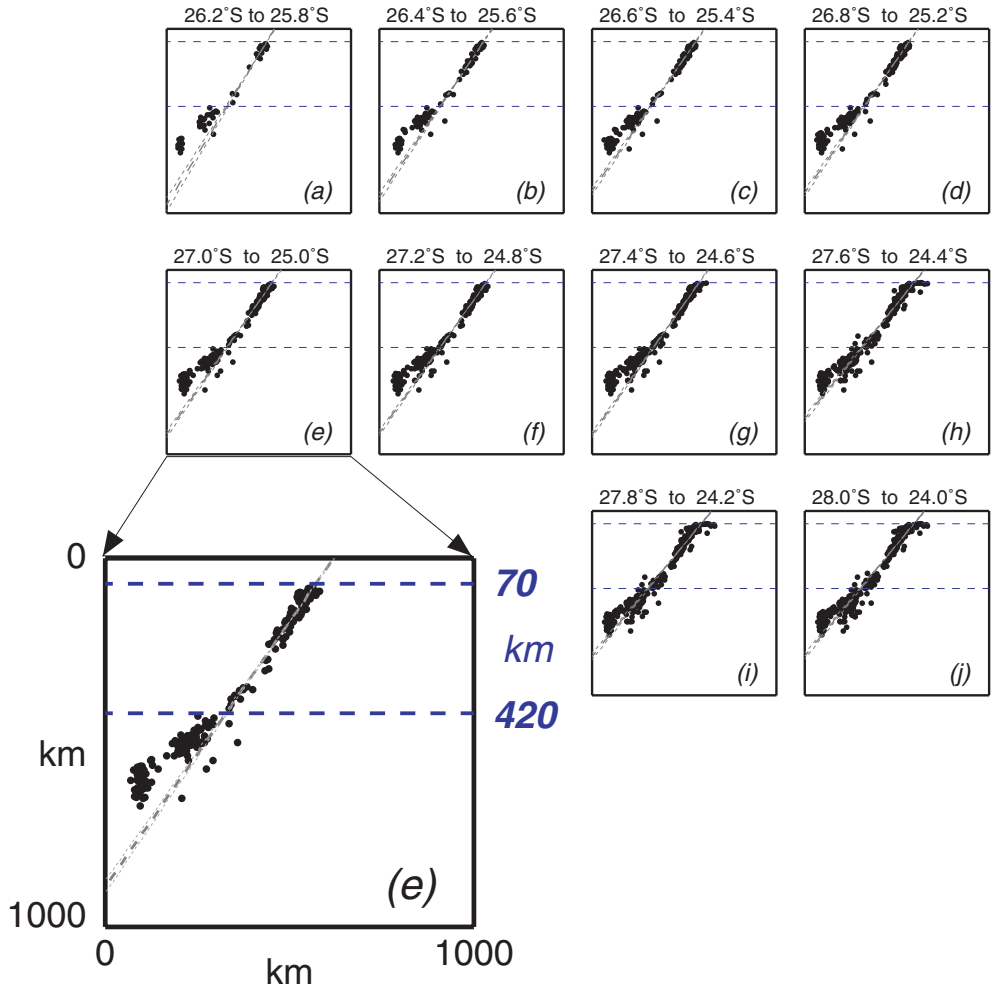

Figure 1. Example of cross-sections of the Tonga Benioff zone, centred at 26°S and involving progressively wider latitudinal bands, from 0.4° width (a) to 4° width (j). In each frame, the solid dots represent the projections of seismicity, from the catalogue of Engdahl *et al.* (1998). The horizontal dashed lines (at 70 and 420 km) bound the depth range over which the best fitting is carried out. The grey dashes show the best linear fits, with the dotted lines representing 1σ deviations. The smallest variance is obtained for a 2°-wide band (e). The enlarged box at bottom left is an enlargement of frame (e).

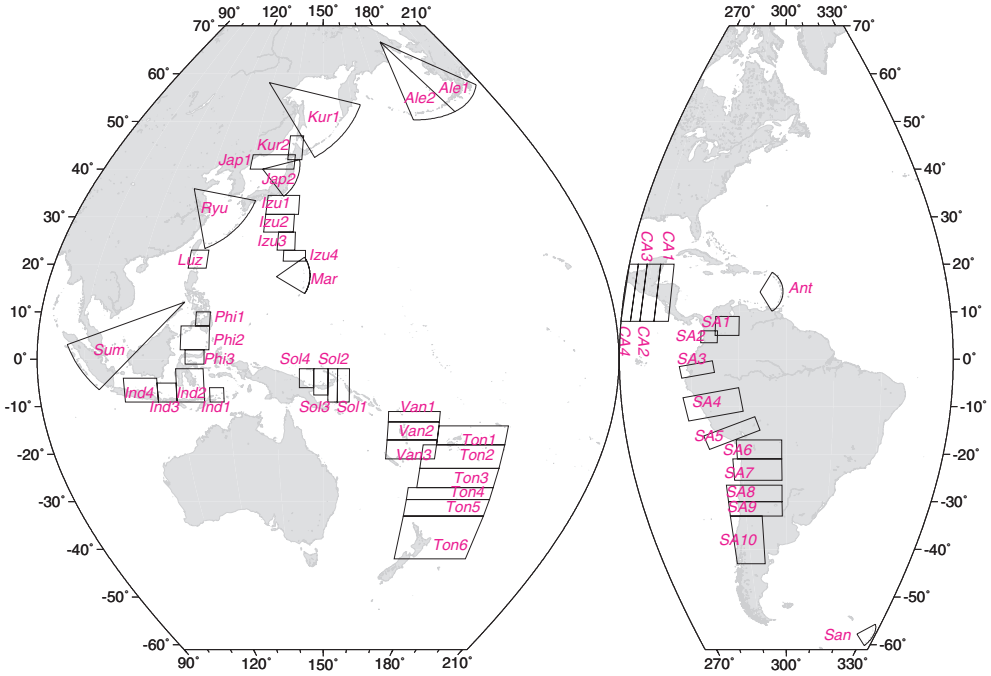

Figure 2. Map of the 50 regions with homogeneous slab dipping characteristics used in the present study, identified by their three- or four-character code. Regions shown as sectors were processed using cylindrical projections.

relocated hypocentres of Engdahl *et al.* (1998) and plot cross-sections of the seismicity centred at a common point along the trench (in this case 26°S) for sub-datasets of increasing width [we start in Fig. 1(a) with a latitudinal band of 0.4°, which we increase by steps of 0.4°, up to 4° in Fig. 1(j)]. At each step, we define a best-fitting strike and dip for the subdata set, following the technique of Chen *et al.* (2001a); the procedure is iterated by discarding obvious outliers (defined as lying more than 3σ from the best-fitting line). The latitudinal band defining the final segmentation (in this case, a 2° width, ranging from 25° to 27°S in Fig. 1(e) and enlarged in the bottom left) is obtained by minimizing the standard deviation σ of the linear fit. The rectangular boxes in Fig. 2 identify the individual subduction segments, or regions used in the present study. Segmentation for South America was adapted directly from Chen *et al.* (2001a). In other regions, it was achieved through the optimization process described in Fig. 1. The final best-fitting cross-sections are regrouped in Fig. 3.

In each subduction zone, we then use the best-fitting strike and dip to define the slab reference frame, and project the *P* and *T* axes of the local CMT solutions following the conventions of Chen *et al.* (2001a), themselves inspired by Vassiliou *et al.* (1984) and Apperson & Frohlich (1987). The data set of focal mechanisms consists of the Harvard CMT catalogue (restricted to centroid depths between 70 and 300 km) from 1976 to 2001, augmented by the results of Chen *et al.* (2001b) from 1962 to 1975 in the depth range 130–300 km. When the depth of a CMT event is beyond the regional depth range selected to invert slab geometry, a different reference dip angle is adopted, to account for the bending of the slab, as expressed by the shape of the Benioff zone.

Upon projection in the slab frame, each event is then characterized as DP if its *P* axis is less than 30° away from the direction of downdip, DT if its *T* axis is such, or ND otherwise. In turn, a geographic grouping of mechanisms, such as a region or a depth interval within a region, is described as being downdip stress-dominant if the total number of its DP and DT events is greater than that of ND events.

3.1 Arcuate trench geometries

Our procedure is slightly different in the case of trenches with significant arc curvatures, shown as sectors on Fig. 2, which warrant the use of cylindrical projections to accommodate the continuing change of strike along the trench. We first invert for the pole whose small circle best fits the curvature of the volcanic arc (Simkin & Siebert 1994). Because of scarce subaerial volcanism in the Ryukyu trench, the pole of that arc is derived by fitting seismicity at depths of 210 to 230 km. In a cylindrical cross-section, the abscissa of an earthquake in the projection plane is its horizontal distance from the pole and its ordinate is simply its depth. The dip angle is again determined by best fitting a straight line to the projections of earthquakes within chosen depth ranges. For each CMT solution, a local slab strike is simply defined as normal to the azimuth of the pole with respect to the epicentre. The rest of the procedure follows that for linear trenches; results are incorporated into Figs 3 and 4.

4 RESULTS

Fig. 4 presents the data set of 1900 focal mechanisms projected onto slab coordinates for the 50 regions, arranged in the same order as on Fig. 3. For each region, the along-strike direction along the unit circle is oriented upwards, the slab-normal direction (with an oceanward component) to the right and the downdip direction inwards at the centre of the circle. The smaller inner circle represents a deviation of 30° from the downdip direction. For events with stresses oriented downdip (DP and DT), we plot the *P* and *T* axes with black circles and diamonds, respectively: one of them always falls inside the inner

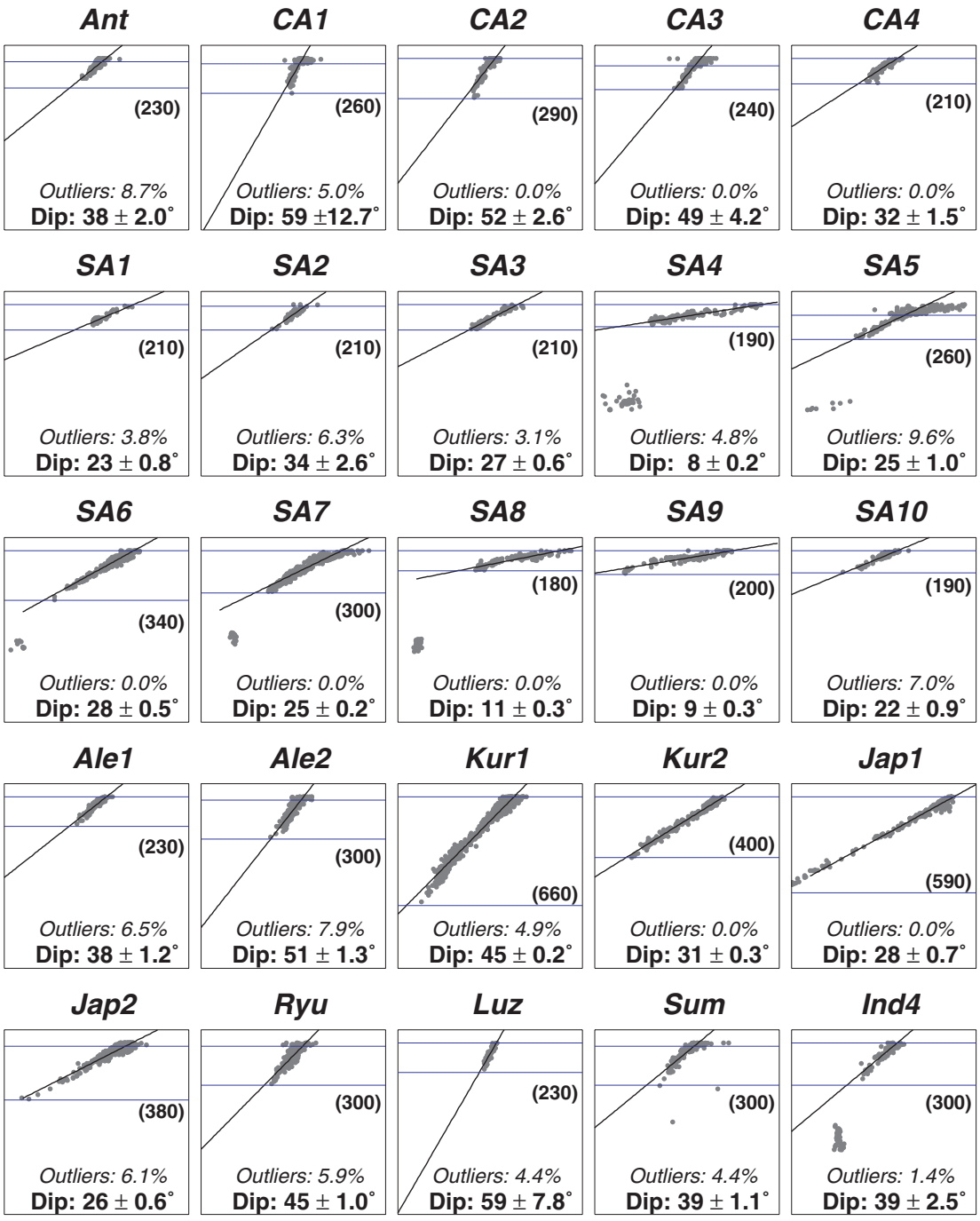

Figure 3. Results of best-fitting of slab geometry in each of the 50 regions under study. Only events (individual grey dots) between the two horizontal lines are used in the regressions. Numbers in parentheses indicate depths (in km) of the lower bound of the fitting interval. Dips shown with 1σ errors in all regions. Outliers eliminated within each fitting depth band are not shown, but their percentage is given.

circle. ND events are plotted using the same symbols, but in grey: we verify that there should be no grey symbols inside the inner circle.

We then use a ternary diagram (Fig. 5) to express the fractions of the populations of CMT solutions belonging to the three categories of mechanisms. This approach is inspired by the ternary representation of focal mechanisms introduced by Frohlich & Apperson (1992). However, it differs in that Frohlich and Apperson use the diagram to plot the stress orientation of single earthquakes, whereas Fig. 5 represents the populations of mechanisms in the various regions, each earthquake being conveniently described as fully DP, DT, or ND. While our diagram and theirs share the same apices in the sense that a population composed entirely of one of Frohlich and Apperson's end-members (pure thrust, pure normal, or pure strike-slip after rotation into slab coordinates) would plot at the same apex on Fig. 5, the converse is not true. For example, a region is 100 per cent DP if all of its earthquakes approach sufficiently a DP mechanism: however, the 30° tolerance introduced in our algorithm means that individual earthquakes in such a family could be somewhat scattered away from the corresponding apex in the representation of Frohlich & Apperson (1992).

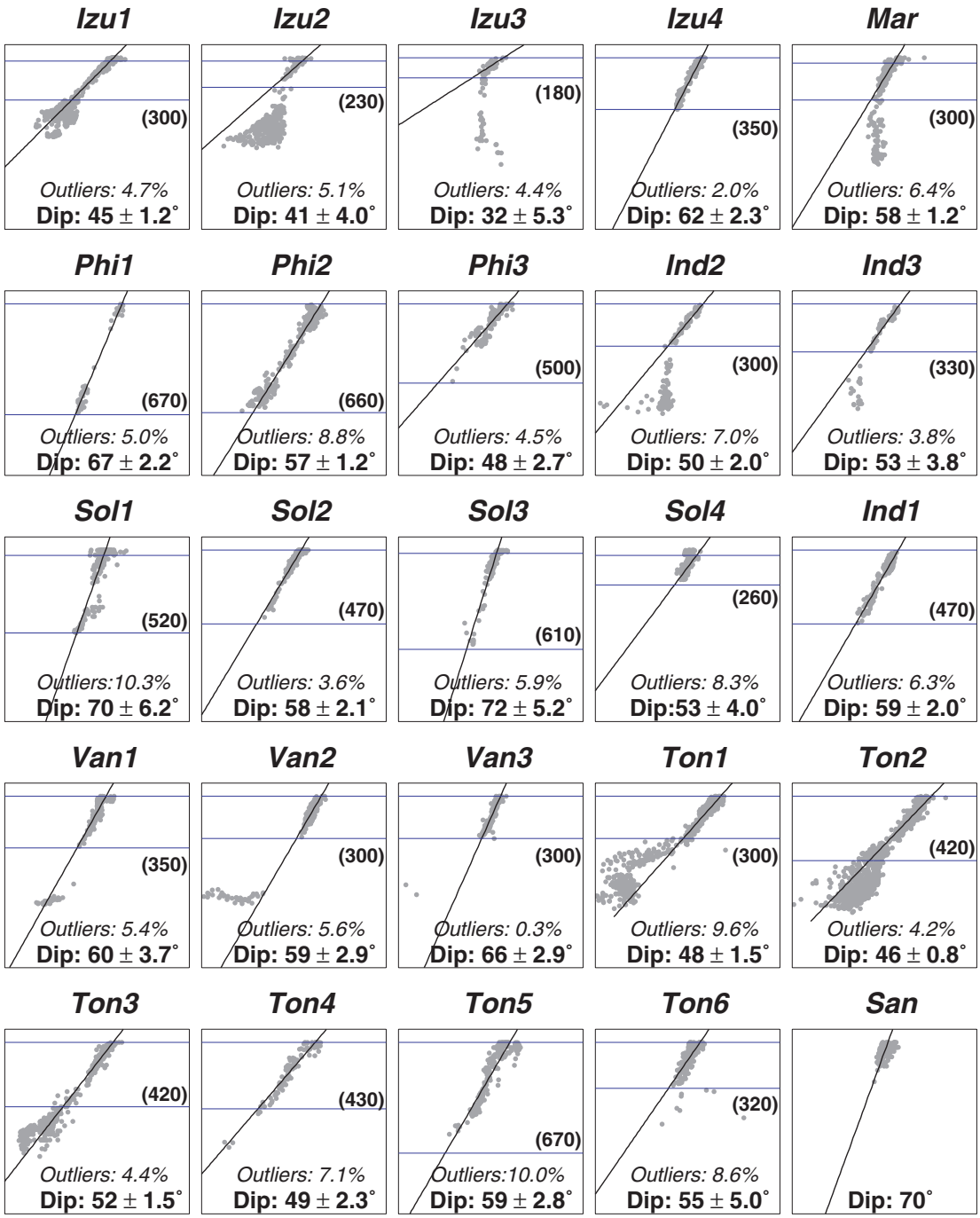

Figure 3. (*Continued.*)

The horizontal dashed line on Fig. 5 is a convenient separation between regions with dominant (below) and non-dominant (above) downdip stress release. The vertical dotted line further separates regions dominated by DP events (to the left) and DT ones (to the right). For both latter regions, we compute thermal parameters Φ (defined as the product of the age of the subducting lithosphere by its vertical rate of descent Kostoglodov 1989; Kirby *et al.* 1991) and colour-code their symbols on Fig. 5. Because of unknown ages for the Solomon Sea plate and the South China sea lithosphere, we leave the symbols for Sol3 and Luz uncoded. For Ind1 and Ind3, we use reduced thermal parameters, computed from the slow GPS convergence rates observed across the Timor trench (Genrich *et al.* 1996).

The following three observations constitute the main results of our compilations of focal mechanisms and, to the best of our knowledge, were not previously identified:

(i) *Orientation of conjugate stresses in DP and DT mechanisms* In regions dominated by downdip stresses (those in the bottom half of Fig. 5), conjugate axes (i.e. *T* axes in DP events and *P* axes in DT events) tend to orient in the slab-normal direction (i.e. the null axes tend to be along the strike of the trench). Examples would be

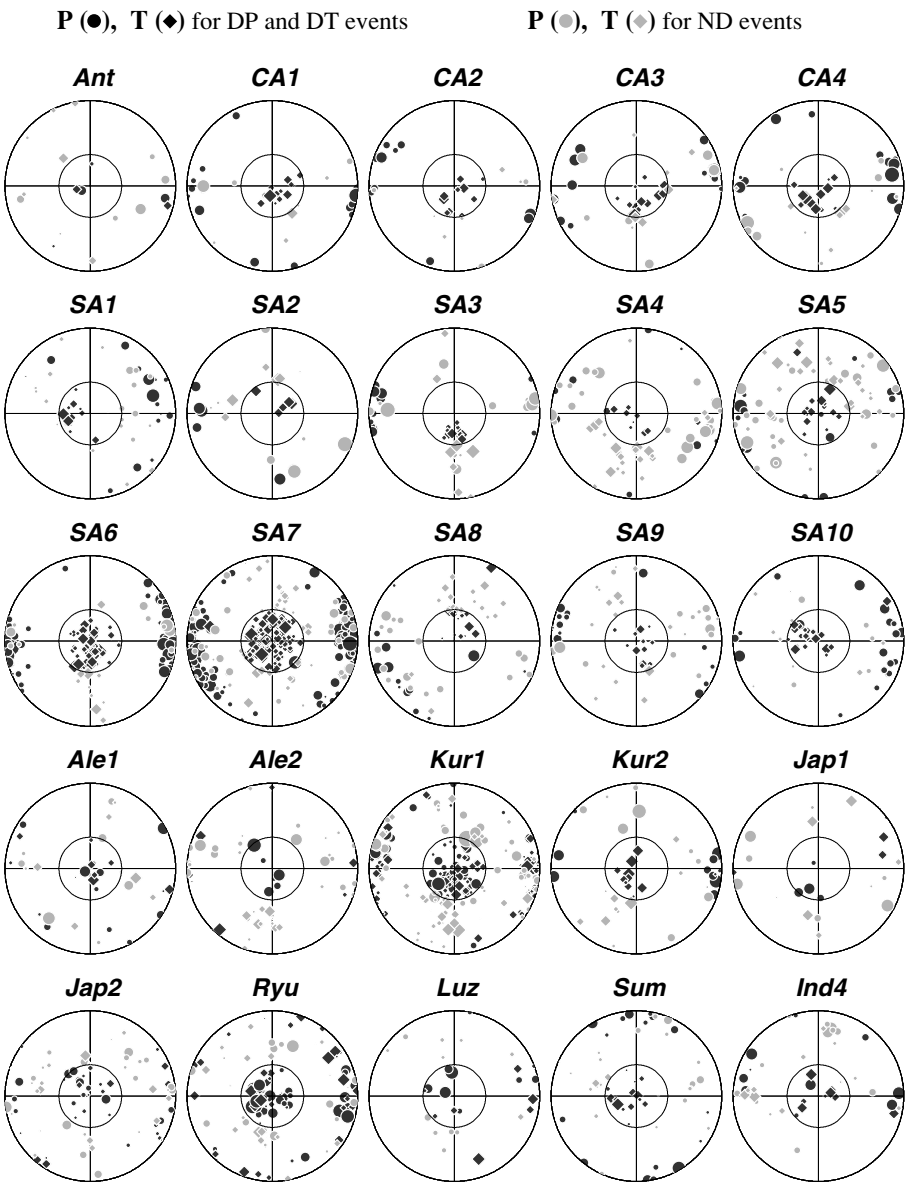

Figure 4. Full data set of *P* and *T* axes of intermediate-depth earthquakes in each of the 50 regions studied. Each diagram is a stereographic projection in the slab reference frame. The trench strike is oriented upwards on the figure and the downdip direction plots at the centre of each circle; the slab-normal direction (with an oceanward component) is to the right. The smaller circle characterizes an angular distance of 30° from the downdip axis. An event is characterized as DP (resp. DT) if its *P*-axis (resp. *T*) falls within the small circle; its axes are then plotted with black symbols. Otherwise, it is characterized as ND and its axes are plotted in grey. The size of symbols is keyed to the moment of the earthquakes. Note the frequent occurrence of black symbols at the 3 and 9 o'clock positions, indicating slab-normal conjugate stresses, suggestive of the reactivation of fossil faults.

regions 2 and 3 in Tonga (Ton2 and Ton3 on Fig. 4) and regions 6 and 7 in South America (SA6 and SA7). The only exceptions to this pattern (4 out of 25 regions) are Sum, Ind1, Ale1 and Van3.

(ii) *Preferential downdip compression in colder slabs*

In regions dominated by downdip stresses, there exists a clear trend of decreasing thermal parameters from left to right; indeed, for the 23 regions listed in Table 1, we find a 78 per cent correlation between log Φ and the difference between the barycentric (triangular) coordinate relative to end-members DP and DT on Fig. 5. This thermal control of downdip stress is corroborated in the Ryukyu and Aleutian trenches (the so-called stress-segmented zones in the nomenclature of Fujita & Kanamori 1981), where the locations of DP and DT events display clear spatial separation, and correlate with older and younger lithospheric ages, respectively (see Fig. 6).

(iii) *Regions not dominated by downdip stresses*

In some regions not dominated by downdip stresses, a significant number of ND events exhibit lateral stresses, i.e. subhorizontal *P* or *T* axes located in the slab plane or close to it. Examples would be the *T* axes in the Mariana and South Sandwich arcs and in part of the Aleutian one (Mar, San and Ale2 on Fig. 4), and the *P* axes in region Tonga 4.

5 DISCUSSION OF PROPOSED MECHANISMS

In the next sections, we examine systematically the various published models for the origin of stresses in intermediate-depth earthquakes. Even though the majority of these models were derived to explain DP or DT geometries (i.e. either *P* or *T* axes oriented

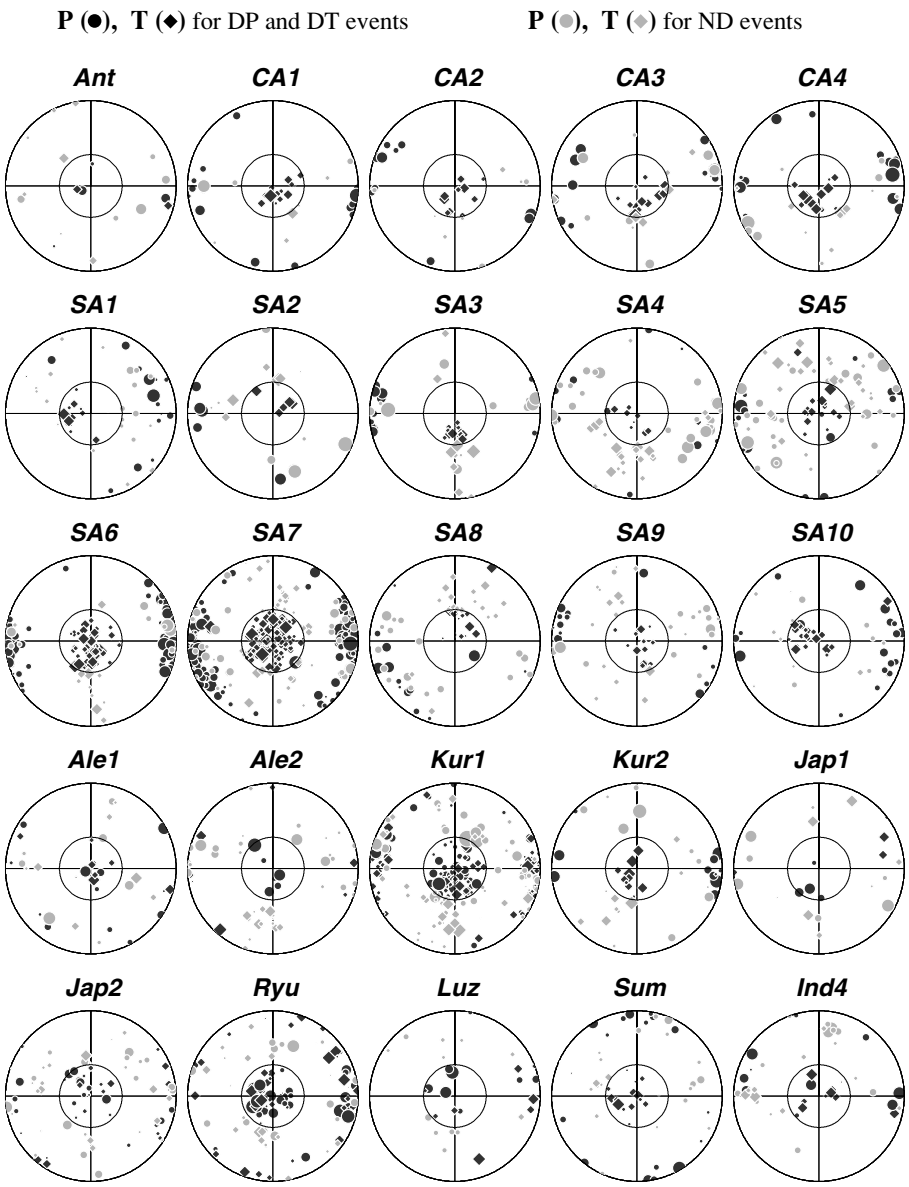

Figure 4. (*Continued.*)

downdip), we will examine their predictions in more detail, for example regarding the orientation of conjugate stresses under DP or DT geometries.

5.1 Assessment of the thermomechanical model

As expected from the model, the majority of regions dominated by DT events (CA1 to CA4, SA1, SA3, SA10, Ale1 and Sum) lack seismicity deeper than 300 km, while SA6, SA7 and Ind3 show seismic gaps between intermediate and deep earthquakes. Deep seismicity under the Fiji plateau (Van1 and Van3) is probably unrelated to subduction at the Vanuatu trench (Okal & Kirby 1998). While seismic activity in Kur2, Ind1 and Ton6 extends deeper than 300 km, it is absent below 500 km, suggesting a lack of penetration into the lower mantle and thus of the resulting DP stresses. Similarly, among regions dominated by DP events, Kur1, Sol3, Ton1, Ton2 and Ton3 display continuous seismicity to depths in excess of 500 km, in agreement with the thermomechanical model.

That leaves Luz and Ryu as violators of the predictions of the model, being short Benioff zones not extending beyond 300 km, but dominated by DP events (Jap2 is a borderline case, with no definite trend in its population, which features a prominent double seismic zone (Kawakatsu & Seno 1983)). While Luzon is a very complex tectonic region, where two subduction zones with opposite polarities compete on either side of the northern part of the island, there is essentially no way to reconcile the observations in the Ryukyu subduction zone with the thermomechanical model, as noted early on by Isacks & Molnar (1971).

An additional shortcoming of the thermomechanical model is that significant seismic gaps between intermediate and deep earthquakes (e.g. in South America or western Java) have been found to occur in mechanically continuous slabs, by investigators using seismic tomography (Engdahl *et al.* 1995) or the unattenuated propagation of high-frequency shear waves (Sacks 1969; Isacks & Barazangi 1973; Okal 2001). If the material is mechanically continuous, it would be expected to transmit stresses, and slabs with seismic gaps should be

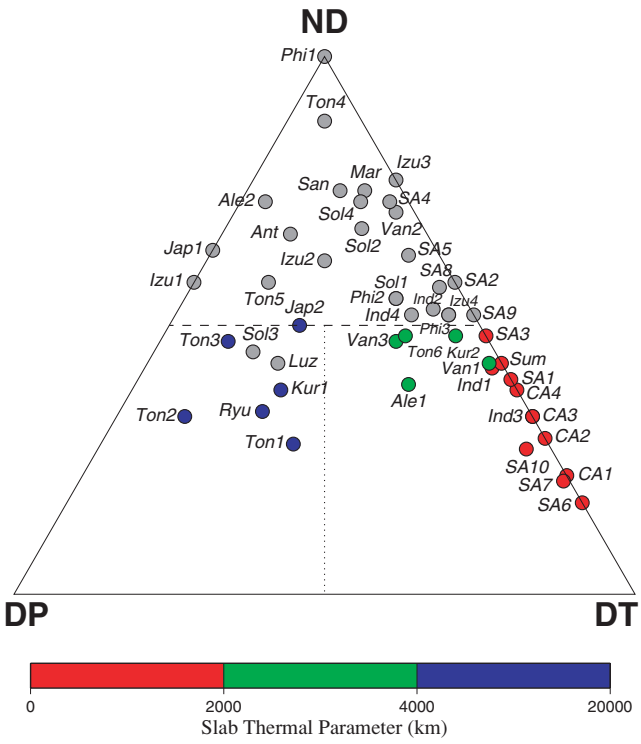

Figure 5. Ternary diagram representing, for each region under study, fractions of the CMT data set characterized as downdip compressional (DP), downdip tensional (DT) or neither (ND). The horizontal dashed line separates those regions dominated or not by downdip stresses, i.e. for which more or less than half of the events are either DP or DT. For the dominated regions, the vertical dotted line separates those in downdip compression (to the left) from those in downdip tension (to the right) and the events are colour-coded according to the thermal parameter Φ listed in Table 1. Sol3 and Luz are plotted in grey, for failure to determine a reliable Φ (see text).

in the same state of stress as those exhibiting deep seismicity, rather than as shorts slabs.

In conclusion, while the thermomechanical model accounts well for first-order differences between significant numbers of DP and DT regions, it does retain substantial shortcomings in a number of specific other environments.

5.2 Assessment of the petrological model

In regions dominated by downdip stresses, the good correlation between the nature (compressional or tensional) of the downdip stress and the thermal parameter Φ [result (ii) above] suggests the predominant role of thermally induced forces in controlling downdip stresses. Although the greater upwarping of the α-phase transition at 410 km and the larger thermal contraction in colder slabs would induce more tensile stresses, result (ii) implies that, in colder and faster slabs, these effects are overpowered by the compressional stress generated by the combination of: (a) the greater downwarping of the perovskite-forming transition at 660 km; (b) the potential presence of metastable olivine; and (c) the inhibition of slab penetration (as a result of buoyancy forces, viscosity contrasts or compositional changes) at the bottom of the transition zone. Furthermore, this model of thermally controlled stress patterns provides a potential explanation for the stress-segmented zonations observed in the Aleutian and Ryukyu arcs by Fujita & Kanamori (1981). Thus, our observations suggest that buoyancy forces associated with thermal

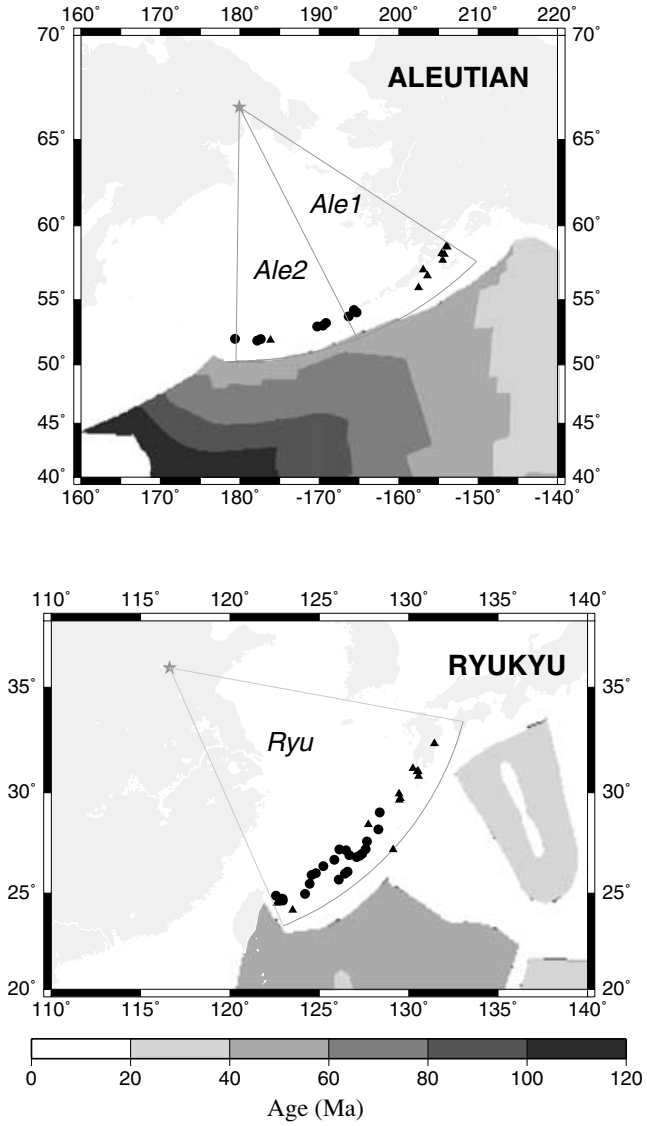

Figure 6. Close-up of DP and DT events in the Aleutian (top) and Ryukyu (bottom) regions. The stars are the poles of the relevant arcs. DP events are plotted as solid circles, DT events as solid triangles. Note the spatial separation between the groups, and the correlation with the age of the subducting lithosphere, shade-coded according to the horizontal bar.

perturbations of petrological phase relations contribute significantly to the downdip stress fields in slabs.

5.3 Assessment of the FK model

Because our results support the concept of thermally controlled downdip stresses, they should then disagree with the model of Fujita & Kanamori (1981) where the age of the slab and the rate of convergence are competitive factors. In order to examine this situation in detail, we plot on Fig. 7 ages and rates for the 23 subduction zones dominated by down-going stresses. We use the same plotting conventions and aspect ratio as in fig. 6 of Fujita & Kanamori (1981). Fundamental differences between the two plots include the following.

(i) Reclassifying (on the basis of a much enlarged data set processed with a more formalized algorithm) many subduction zones

Table 1. Geometric and kinematic parameters of selected subduction zones.

Region	Depth interval used for best fit (km)	Best-fitting plane strike (°)	Best-fitting plane dip (°)	Age at trench (Ma)	Age at trench Ref.	Parameters of convergence: Plate or block pair	Rate (mm yr^{-1})	Thermal parameter Φ (km)	Ref.
Central America									
CA1	70–470	312	59	17	a	COC-CAR	79	1200	b
CA2	70–290	291	52	16	a	COC-CAR	73	900	b
CA3	110–240	307	49	16	a	COC-NAM	76	900	b
CA4	70–210	311	32	15	a	COC-NAM	70	600	b
South America									
SA1	70–210	12	23	20	a	NAZ-SAM	57	400	b
SA3	70–210	294	27	20	a	NAZ-SAM	36	300	b
SA6	70–340	338	28	44	a	NAZ-SAM	77	1600	b
SA7	70–300	355	25	44	a	NAZ-SAM	79	1500	b
SA10	70–190	15	22	30	a	NAZ-SAM	77	1600	b
Aleutian, Kuriles, Japan, Ryukyu									
Ale1	70–230	234	38	53	a	PAC-NAM	62	2000	b
Kur1	70–660	218	45	100	c	PAC-NAM	80	5700	b
Kur2	70–400	253	31	130	a	PAC-NAM	57	3800	b
Jap2	90–380	190	26	130	a	PAC-EUR	90	5100	b
Ryu	70–230	228	45	59	a	PHL-EUR	111	4700	d
Indonesia									
Sum	90–300	330	39	50	a	AUS-SUN	28	900	e
Ind3	70–330	271	53	144	a	AUS-TIM	<10	<2000	f
Ind1	70–470	244	59	140	g	AUS-TIM	<10	<2000	f
Vanuatu									
Van1	70–350	350	60	28	h	AUS-PAC	96	2300	b
Van3	70–300	336	66	50	h	AUS-PAC	78	3600	b
Tonga									
Ton1	70–300	186	48	110	c	PAC-LAU	238	19500	i
Ton2	70–420	202	46	110	c	PAC-LAU	163	12900	i
Ton3	70–420	189	52	100	h	PAC-AUS	68	5400	b
Ton6	70–320	217	55	100	g	PAC-AUS	33	2700	b

References: (a) Müller *et al.* (1997); (b) DeMets *et al.* (1994); (c) Wiens & Gilbert (1996); (d) Kimura (1985), Seno *et al.* (1993); (e) Rangin *et al.* (1999); (f) Genrich *et al.* (1996); (g) this study; (h) Gorbatov & Kostoglodov (1997); (i) Bevis *et al.* (1995).
Plate and block abbreviations: Australia (AUS); Caribbean (CAR); Cocos (COC); Eurasia (EUR); Lau basin (LAU); North America (NAM); Nazca (NAZ); Pacific (PAC); Philippines (PHL); South America (SAM); Sunda block (SUN); Timor block (TIM).

as dominated by ND events (plotting towards the apex of Fig. 5) and thus not including them as either DP or DT on Fig. 7. This would be the case of San (South Sandwich islands; Scotia trench in FK) or Ale2 (Alaska in FK).

(ii) Using better constrained convergence rates, especially in the case of decoupled blocks such as the Lau basin (Bevis *et al.* 1995) or of the subduction of the Philippine Sea Plate (which has no spreading centre) under the Ryukyu trench. In this latter case, we use a convergence rate of 11 cm yr^{-1} (Seno *et al.* 1993), more than double that used by Fujita & Kanamori (1981), and in general agreement with both the 8 cm yr^{-1} predicted by Sella *et al.* (2002) between the Philippine sea and China sea solid blocks, and the 4 cm yr^{-1} of backarc spreading reported by Kimura (1985) in the Okinawa trough.

As a result of the elimination of Ale2 and San, and of the revision of the convergence rate for Ryu, the data set plotted on Fig. 7 no longer features a DP regime for young and slow slabs. Rather, it suggests that the influence of age and rate are complementary, and generally supports the thermomechanical and petrological models.

Finally, among slabs reported as fast and young by Fujita & Kanamori (1981), we also note a significant scatter in the dip of the slab, which varies from very shallow in South America to intermediate in Central America and steep in Vanuatu (see Fig. 1). This cannot support loading by the overriding plate as the source of the DT mechanisms observed in those environments.

5.4 Assessment of the ping-pong model

We recall that this model (Frank 1968; Tovish & Schubert 1978) predicts an influence of the curvature of the arc on the nature of lateral stresses, i.e. principal stresses oriented subhorizontally and lying approximately in the subducting plane. In order to assess the performance of the model, we consider regions not dominated by downdip stresses (the top half of Fig. 4) and we focus on their ND events. We use a second ternary diagram in Fig. 8 to plot the fraction of the population of ND events in each region that is in lateral compression, i.e. whose *P*-axis is within 15° of the slab plane, in lateral tension (*T* similarly oriented), or neither. Furthermore, we colour-code Fig. 8 according to the quantity $\delta/2$—RC, which could be called the ping-pong misfit, and that should predict lateral stresses in the slab (Isacks & Molnar 1971).

The important results from Fig. 8 are as follows. First, those regions with a strong positive ping-pong misfit are found to be in lateral tension, as predicted by the model. These are regions where the RC angle is small, i.e. the curvature important, and these develop a strong lateral extension. Secondly, the correlation is less good for

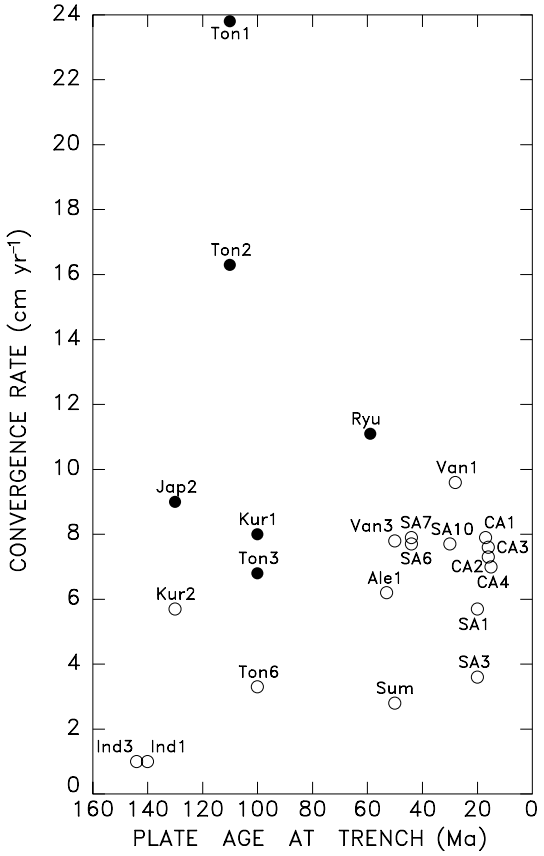

Figure 7. Trench-normal convergence rate plotted as a function of the age of the subducting lithosphere, for the 23 regions dominated by downdip stresses. Open circles are used for downdip tensional (DT) regions, solid circles for downdip compressional (DP) ones. To allow direct comparison, this plot uses the same conventions (including the reversed horizontal scale) and the same aspect ratio as fig. 6 of Fujita & Kanamori (1981).

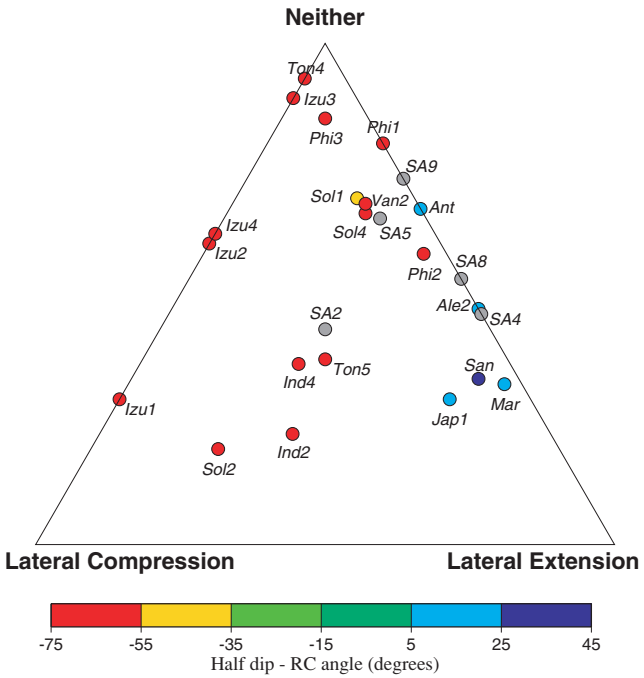

Figure 8. Ternary diagram representing, in the 27 regions not dominated by downdip stresses, the fractions of the ND event population featuring lateral compression (i.e. their *P*-axis within 15° of the slab), lateral tension (same for the *T*-axis), or neither. The symbols are colour-coded by the value of the ping-pong misfit, defined as the difference between the half-dip of the slab and the RC angle. Note that regions with strong positive ping-pong misfit are under lateral tension, as predicted by the ping-pong model.

compressional events: while ND events with strong lateral compression occur only in regions of negative ping-pong misfit, the converse is not true and such regions can sustain events with neither lateral stress. This should not be taken as a failure of the model, because these regions have a large RC angle and hence little curvature, so one would not expect much influence from membrane stresses in the first place. More significant perhaps is the lack of ND events in regions with zero or small ping-pong misfit. If the slab is essentially unstretched, it contributes no membrane stresses and the principal stresses have a better chance of being downdip, either DP or DT.

In conclusion, the ping-pong model correctly predicts the tensile lateral stresses in regions with strong curvature, such as San, Mar, Ale2 and Jap1.

5.5 Assessment of the influence of reactivation of fossil faults

In order to test this suggestion, we assume the existence of a fossil fault, whose geometry is inspired by that of outer-rise earthquakes, as suggested in fig. 1 of Jiao *et al.* (2000). We then consider all possible orientations of seismic slip on such a fault and project the resulting *P* and *T* axes using slab coordinates (Fig. 9). When rake approaches 90° (resp. 270°), the *P*-axis (resp. *T*-axis) approaches the downdip axis, with the conjugate *T*-axis (resp. *P*) approaching slab-normal orientation, i.e. plotting along the right edge of the unit circle in slab coordinates. This is in excellent agreement with the observation listed as result (i), and we conclude that fossil faults may play a significant role in the genesis of intermediate-depth earthquakes. However, other stress patterns in Fig. 4 are not reproduced on Fig. 9 and this suggests that this reactivation mechanism is not a necessary condition for the origin of intermediate-depth seismicity.

6 CONCLUSION

In summary, contrary to the predictions of the FK model, we find that lithospheric age and subduction rate appear to play complementary, rather than competitive, roles in determining the stress patterns expressed by intermediate-depth seismicity. This is consistent with both the thermomechanical and the petrological buoyancy models. Indeed, in a sense, the latter is a refinement of the former, in that the latter posits that continuation of the slab to greater depths (rather than strictly its seismicity, as in the former) allows it to encounter positive buoyancy anomalies (induced by thermally downwarped perovskite-forming reactions) at depths below the occurrence of negative buoyancy anomalies (induced by thermally upwarped spinel-forming reactions). The magnitudes of these deep-seated positive buoyancy anomalies would then control the extent to which the consequent DP stress regimes propagate updip along slabs toward intermediate depths. The case of the Ryukyu subduction thus poses an interesting question. Tomographic results do not allow an unambiguous detection of the mechanical slab below the apparent seismic cutoff at 300 km (e.g. Lebedev *et al.* 1997; Widiyantoro *et al.* 1999). If the slab does penetrate deeper, then the evident downdip compression at intermediate depths may reflect updip propagation of a deep compressional stress field associated with positive buoyancy

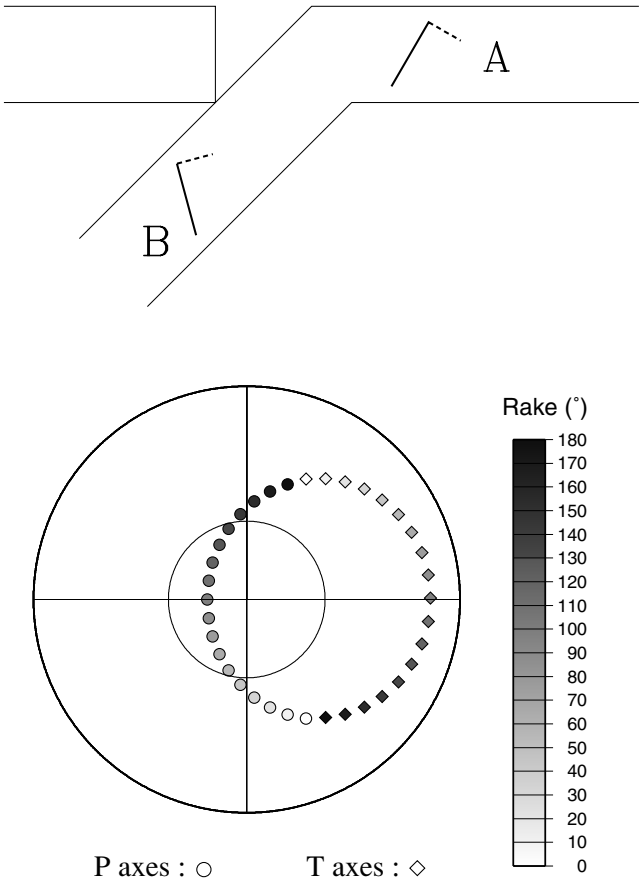

Figure 9. Fossil faults as possible sources of intermediate earthquakes. (Top) Geometry of the model, after Fig. 1 of Jiao *et al.* (2000). The solid trace at location *A* represents the fault of a typical outer-rise earthquake and the dashed line the conjugate fault plane. *B* represents the fossil fault, after rotation at the trench and subduction. (Bottom) Simulation of all possible patterns of *P* (circles) and *T* (diamonds) axes for earthquakes occurring on a fossil fault such as *B* and with rakes varying from 0° to 170° in steps of 10° (for rakes between 180° and 360° simply permute the circles and diamonds). Note that the patterns observed on the majority of diagrams on Fig. 4 are closely matched by rakes of ∼90° (or ∼270°).

forces arising in cold slab material near 600 km. On the other hand, if the slab does not extend significantly below 300–400 km, any positive buoyancy forces giving rise to downdip compression at intermediate depths would more likely be attributable to metastable persistence of buoyant (untransformed) olivine material at those depths.

While these observations focus primarily upon the downdip component of stress patterns, our observations of other components also offer some insight. The ping-pong model appears to be successful in relating the degree of arc curvature to the presence of lateral extensional stresses. Furthermore, observed stress patterns seem to be consistent with the reactivation of fossil outer-rise faults playing a meaningful but not exclusive role in contributing to the stress orientations expressed by intermediate-depth seismicity.

ACKNOWLEDGMENTS

We thank Luciana Astiz, Shoichi Yoshioka and Editor Rob van der Hilst for constructive comments on the original manuscript. This research was supported by the National Science Foundation, under Grant EAR-97-06152.

REFERENCES

Apperson, K.D. & Frohlich, C., 1987. The relationship between Wadati-Benioffzone geometry and *P*, *T*, and *B* axes of intermediate and deep focus earthquakes, *J. geophys. Res.,* **92,** 13 821–13 831.

Astiz, L., Lay, T. & Kanamori, H., 1988. Large intermediate-depth earthquakes and the subduction process, *Phys. Earth planet. Int.,* **53,** 80–166.

Bevis, M., 1986. The curvature of Wadati-Benioff zones and the torsional rigidity of the subducting plates, *Nature,* **323,** 52–53.

Bevis, M. *et al.*, 1995. Geodetic observations of very rapid convergence and backarc extension in the Tonga arc, *Nature,* **374,** 249–251.

Bina, C.R., 1996. Phase transition buoyancy contributions to stresses in subducting lithosphere, *Geophys. Res. Lett.,* **23,** 3563–3566.

Bina, C.R., 1997. Patterns of deep seismicity reflect buoyancy stresses due to phase transitions, *Geophys. Res. Lett.,* **24,** 3301–3304.

Bina, C.R., Stein, S., Van Ark, E.M. & Marton, F.C., 2001. Implications of slab mineralogy for subduction dynamics, *Phys. Earth planet. Int.,* **127,** 51–66.

Chen, P.-F., Bina, C.R. & Okal, E.A., 2001a. Variations in slab dip along the subducting Nazca plate, as related to stress patterns and moment release of intermediate-depth seismicity, and to surface volcanism, *Geochem., Geophys., Geosyst.,* **2,** 2001GC000153, 18pp (electronic journal).

Chen, P.-F., Nettles, M., Okal, E.A. & Ekström, G., 2001b. Centroid Moment Tensor solutions for intermediate-depth earthquakes of the WWSSN-HGLP era (1962–1975), *Phys. Earth planet. Int.,* **124,** 1–7.

Creager, K.C., Chiao, L.-Y., Winchester, J.P. & Engdahl, E.R., 1995. Membrane strain rates in the subducting plate beneath South America, *Geophys. Res. Lett.,* **22,** 2321–2324.

Davies, G.F., 1980. Mechanics of subducted lithosphere, *J. geophys. Res.,* **85,** 6304–6318.

DeMets, D.C., Gordon, R.G., Argus, D.F. & Stein, S., 1994. Effect of recent revisions to the geomagnetic reversal time scale on estimates of current plate motions, *Geophys. Res. Lett.,* **21,** 2191–2194.

Dziewonski, A.M., Friedman, A., Giardini, D. & Woodhouse, J.H., 1983. Global seismicity of 1982: centroid-moment-tensor solutions for 308 earthquakes, *Phys. Earth planet. Int.,* **33,** 76–90.

Engdahl, E.R. & Scholz, C.H., 1977. A double Benioff zone beneath the central Aleutians: An unbending of the lithosphere, *Geophys. Res. Lett.,* **4,** 473–476.

Engdahl, E.R., van der Hilst, R.D. & Berrocal, J., 1995. Imaging of subducted lithosphere beneath South America, *Geophys. Res. Lett.,* **22,** 2317–2320.

Engdahl, E.R., van der Hilst, R.D. & Buland, R.P., 1998. Global teleseismic earthquake relocation with improved travel-time and procedures for depth determination, *Bull. seism. Soc. Am.,* **88,** 722–743.

Engebretson, D.C. & Kirby, S.H., 1992. Deep Nazca slab seismicity: why is it so anomalous?, *EOS, Trans. Am. geophys. Un.,* **73**(43), 379 (abstract).

Frank, F.C., 1968. Curvature of island arcs, *Nature,* **220**, 363.

Frohlich, C. & Apperson, K.D., 1992. Earthquake focal mechanisms, moment tensors, and the consistency of seismic activity near plate boundaries, *Tectonics,* **11,** 279–296.

Fujita, K. & Kanamori, H., 1981. Double seismic zones and stresses of intermediate-depth earthquakes, *Geophys. J. R. astr. Soc.,* **66,** 131–156.

Genrich, J.F., Bock, Y., McCaffrey, R., Calais, E., Stevens, C.W. & Subarya, C., 1996. Accretion of the Southern Banda arc to the Australian plate margin determined by Global Positioning System measurements, *Tectonics,* **15,** 288–295.

Gorbatov, A. & Kostoglodov, V., 1997. Maximum depth of seismicity and thermal parameter of the subducting slab, *Tectonophysics,* **277,** 165–187.

Goto, K., Hamaguchi, H. & Suzuki, Z., 1983. Distribution of stress in descending plate in special reference to intermediate and deep focus earthquakes, I. Characteristic of thermal stress distribution, *Tohoku Geophys. J.,* **29,** 81–105.

Goto, K., Hiroyuki, H. & Suzuki, Z., 1985. Earthquake generating stresses in a descending slab, *Tectonophysics,* **112,** 111–128.

Goto, K., Suzuki, Z. & Hamaguchi, H., 1987. Stress distribution due to olivine-spinel phase transition in descending plate and deep focus earthquakes, *J. geophys. Res.,* **92,** 13 811–13 820.

Green, H.W., , II & Houston, H., 1995. The mechanics of deep earthquakes, *Ann. Revs. Earth planet Sci.,* **23,** 169–213.

Guest, A., Schubert, G. & Gable, C.W., 2003. Stress field in the subducting lithosphere and comparison with deep earthquakes in Tonga, *J. geophys. Res.,* **108**(B6), 2288, doi:10.1029/2002JB002161. (**ETG-4,** 16pp).

Hamaguchi, H., Goto, K. & Suzuki, Z., 1983. Double-planed structure of intermediate-depth seismic zone and thermal stress in the descending plane, *J. Phys. Earth,* **31,** 329–347.

House, L.S. & Jacob, K.H., 1982. Thermal stresses in subducting lithosphere can explain double seismic zones, *Nature,* **295,** 587–589.

Isacks, B.L. & Barazangi, M., 1973. High frequency shear waves guided by a continuous lithosphere descending beneath Western South America, *Geophys. J. R. astr. Soc.,* **33,** 129–139.

Isacks, B.L. & Molnar, P., 1971. Distribution of stresses in the descending lithosphere from a global survey of focal mechanism solutions of mantle earthquakes, *Revs. Geophys. Space Phys.,* **9,** 103–174.

Jiao, W., Silver, P.G., Fei, Y. & Prewitt, C.T., 2000. Do intermediate- and deep-focus earthquakes occur on pre-existing weak zones? An examination of the Tonga subduction zone, *J. geophys. Res.,* **105,** 28 125–28 138.

Kao, H. & Chen, W.-P., 1994. Double seismic zone in Kuril-Kamchatka: the tale of two overlapping single seismic zones, *J. geophys. Res.,* **99,** 6913–6930.

Kao, H. & Liu, L., 1995. A hypothesis for the seismogenesis of double seismic zones, *Geophys. J. Int.,* **123,** 71–84.

Kawakatsu, H., 1985. Double seismic zones: A first order feature of plate tectonics, *PhD thesis,* Stanford Univ., Stanford.

Kawakatsu, H. & Seno, T., 1983. Triple seismic zone and the regional variation of seismicity along the Northern Honshu arc, *J. geophys. Res.,* **88,** 4215–4230.

Kimura, M., 1985. Back-arc rifting in the Okinawa Trough, *Mar. Petrol. Geol.,* **2,** 222–240.

Kirby, S.H., Durham, W.B. & Stern, L.A., 1991. Mantle phase changes and deep-earthquake faulting in subducting lithosphere, *Science,* **252,** 216–225.

Kostoglodov, V.V., 1989. Maximum depth of earthquakes and phase transitions in the lithosphere descending into the mantle, in *Physics and internal structure of the Earth,* pp. 52–57, ed. Magnitskii, V.A., Nauka, Moscow (in Russian).

Lay, T., Astiz, L., Kanamori, H. & Christensen, D.H., 1989. Temporal variation of large intraplate earthquakes in coupled subduction zones, *Phys. Earth planet. Int.,* **54,** 258–312.

Lebedev, S., Nolet, G. & van der Hilst, R.D., 1997. The upper mantle beneath the Philippine Sea region from waveform inversion, *Geophys. Res. Lett.,* **24,** 1851–1854.

Lundgren, P.R. & Giardini, D., 1992. Seismicity, shear failure and modes of deformation in deep subduction zones, *Phys. Earth planet. Int.,* **74,** 63–74.

Müller, R.D., Roest, W.R., Royer, J.-Y., Gahagan, L.M. & Sclater, J.G., 1997. Digital isochrons of the world's ocean floor, *J. geophys. Res.,* **102,** 3211–3214.

Okal, E.A., 2001. 'Detached' deep earthquakes: Are they really?, *Phys. Earth planet. Int.,* **127,** 109–143.

Okal, E.A. & Kirby, S.H., 1998. Deep Earthquakes beneath the North and South Fiji Basins, SW Pacific: Earth's most intense deep seismicity in stagnant slabs, *Phys. Earth planet. Int.,* **109,** 25–63.

Rangin, C.X., Le Pichon, X., Mazzotti, S., Pubellier, M., Chamot-Rooke, N., Aurelio, M., Walpersdof, A. & Quebral, R., 1999. Plate convergence measured by GPS across the Sundaland/Philippine Sea Plate deformed boundary: the Philippines and Eastern Indonesia, *Geophys. J. Int.,* **139,** 296–316.

Richter, F.M., 1979. Focal mechanisms and seismic energy release of deep and intermediate earthquakes in the Tonga-Kermadec region, and their bearing on the depth extent of mantle flow, *J. geophys. Res.,* **84,** 6783–6795.

Sacks, I.S., 1969. Distribution of absorption of shear waves in South America and its tectonic significance, *Yearbook Carnegie Inst. Washington,* **67,** 339–344.

Samowitz, I.R. & Forsyth, D.W., 1981. Double seismic zone beneath the Mariana Island arc, *J. geophys. Res.,* **86,** 7013–7021.

Sella, G.F., Dixon, T.H. & Mao, A., 2002. REVEL: a model from recent plate velocities from space geodesy, *J. geophys. Res.,* **107**(B4), 10.1029/2000JB000033. (**ETG-11,** 32pp).

Seno, T., Stein, S. & Gripp, A.E., 1993. A model for the motion of the Philippine Sea consistent with NUVEL-1, *J. geophys. Res.,* **98,** 17 941–17 948.

Simkin, T. & Siebert, L., 1994. *Volcanoes of the world,* Geoscience Press, Tucson.

Sleep, N.H., 1979. The double seismic zone in downgoing slabs and the viscosity of the mesosphere, *J. geophys. Res.,* **84,** 4565–4571.

Sykes, L.R., 1966. Seismicity and deep structure of island arcs, *J. geophys. Res.,* **71,** 2981–3006.

Tovish, A. & Schubert, G., 1978. Island arc curvature, velocity of convergence and angle of subduction, *Geophys. Res. Lett.,* **5,** 329–332.

Tsukahara, H., 1980. Physical conditions for double seismic planes of the deep seismic zone, *J. Phys. Earth,* **28,** 1–15.

Umino, N. & Hasegawa, A., 1975. On the two-layered structure of deep seismic plane in norheastern Japan, *Zisin,* **27,** 125–139 (in Japanese).

Vassiliou, M.S. & Hager, B.H., 1988. Subduction zone earthquakes and stress in slabs, *Pure appl. Geophys.,* **128,** 547–624.

Vassiliou, M.S., Hager, B.H. & Raefsky, A., 1984. The distribution of earthquakes with depth and stress in subducting slabs, *J. Geodyn.,* **1,** 11–28.

Veith, K., 1974. The relationship of island arc seismicity to plate tectonics, *PhD thesis,* Southern Methodist Univ., Dallas.

Widiyantoro, S., Kennett, B.L.N. & van der Hilst, R.D., 1999. Seismic tomography with *P* and *S* data reveals lateral variations in the rigidity of deep slabs, *Earth planet. Sci. Lett.,* **173,** 91–100.

Wiens, D.A. & Gilbert, H.J., 1996. Effect of slab temperature on deep-earthquake aftershock productivity and magnitude-frequency relations, *Nature,* **384,** 153–156.

Yamasaki, T. & Seno, T., 2003. Double seismic zone and dehydration embrittlement of the subducting slab, *J. geophys. Res.,* **108**(B4), 2212, doi:10.1029/2002JB001918. (**ESE-4,** 21pp).

Yoshioka, S. & Wortel, M.J.R., 1995. Three-dimensional numerical modeling of detachment of subducted lithosphere, *J. geophys. Res.,* **100,** 20 223–20 244.

Yoshioka, S., Dässler, R. & Yuen, D.A., 1997. Stress fields associated with metastable phase transitions in descending slabs and deep-focus earthquakes, *Phys. Earth planet. Int.,* **104,** 345–361.

Zhou, H.-W., 1990. Observations on earthquake stress axes and seismic morphology of deep slabs, *Geophys. J. Int.,* **103,** 377–401.